Large Polarons as Key Quasiparticles in $SrTiO_3$ and $SrTiO_3$-Based Heterostructures

Andrey Geondzhian,[1] Alessia Sambri,[2] Gabriella M. De Luca,[3,2] Roberto Di Capua,[3,2] Emiliano Di Gennaro,[3,2] Davide Betto,[1,†] Matteo Rossi,[4,5] Ying Ying Peng,[4,6] Roberto Fumagalli,[4] Nicholas B. Brookes,[1] Lucio Braicovich,[1,4] Keith Gilmore,[1,7] Giacomo Ghiringhelli,[4,8] and Marco Salluzzo[2,*]

[1]*ESRF—The European Synchrotron, 71 Avenue des Martyrs, CS 40220, F-38043 Grenoble, France*
[2]*CNR-SPIN Complesso Monte-Santangelo via Cinthia, I-80126 Napoli, Italy*
[3]*Dipartimento di Fisica "Ettore Pancini" Università di Napoli "Federico II", Complesso Monte-Santangelo via Cinthia, I-80126 Napoli, Italy*
[4]*Dipartimento di Fisica, Politecnico di Milano, Piazza Leonardo da Vinci 32, I-20133 Milano, Italy*
[5]*Stanford Institute for Materials and Energy Sciences, SLAC National Accelerator Laboratory, 2575 Sand Hill Road, Menlo Park, California 94025, USA*
[6]*International Center for Quantum Materials,School of Physics, Peking University, Beijing 100871, China*
[7]*Condensed Matter Physics and Materials Science Division, Brookhaven National Laboratory, Upton, New York 11973-5000, USA*
[8]*CNR-SPIN, Piazza Leonardo da Vinci 32, I-20133 Milano, Italy*

(Received 4 May 2020; revised 26 July 2020; accepted 14 August 2020; published 15 September 2020)

Despite its simple structure and low degree of electronic correlation, $SrTiO_3$ (STO) features collective phenomena linked to charge transport and, ultimately, superconductivity, that are not yet fully explained. Thus, a better insight into the nature of the quasiparticles shaping the electronic and conduction properties of STO is needed. We studied the low-energy excitations of bulk STO and of the $LaAlO_3/SrTiO_3$ two-dimensional electron gas (2DEG) by Ti L_3 edge resonant inelastic x-ray scattering. In all samples, we find the hallmark of polarons in the form of intense dd + phonon excitations, and a decrease of the LO3-mode electron-phonon coupling when going from insulating to highly conducting STO single crystals and heterostructures. Both results are attributed to the dynamic screening of the large polaron self-induced polarization, showing that the low-temperature physics of STO and STO-based 2DEGs is dominated by large polaron quasiparticles.

DOI: 10.1103/PhysRevLett.125.126401

After the discovery of a high mobility and superconducting two-dimensional electron gas (2DEG) at the $LaAlO_3/SrTiO_3$ (LAO/STO) interface [1,2], and of high-T_c superconductivity in $CaCuO_2/SrTiO_3$ [3] and $FeSe/SrTiO_3$ [4–6] bilayers, work on bulk and surface electronic properties of STO received renewed interest. Despite a simple band structure, the normal and superconducting properties of STO and STO-based heterostructures are not yet fully understood. In the bulk, the $3d$-Ti t_{2g} ($3d_{xy}$, $3d_{xz}$, $3d_{yz}$) manifold [Fig. 1(a)] forms three uppermost bands characterized by heavy and light effective masses along the primitive lattice vectors [7,8]. Spin-orbit coupling (SOC) removes the degeneracy, and the sixfold t_{2g} bands are split by about 30 meV in a Γ_7^+ doublet and a Γ_8^+ quartet [8]. These new bands, formed by the mixing of atomic $3d$-Ti t_{2g} states, still partially retain their overall orbital character [Fig. 1(a)]. The band hierarchy is reversed, due to confinement, in the 2DEG at the (001) LAO/STO interface [9,10], where bands with prevalent $3d_{xy}$ orbital character are lower in energy.

Optical spectroscopy [11], transport studies [12], and angle-resolved photoemission (ARPES) [13] on Nb-doped STO showed that the carrier effective mass is usually larger than the free electron value and decreases with doping, reaching the nonrenormalized value only at electron density $n_{3D} \gg 10^{20}$ cm^{-3}. Rather than by band filling, this phenomenon was attributed to the coupling of electrons to optical phonon modes, which results in the formation of large polarons [14]. Although most of the features observed in the optical conductivity spectra can be explained by a large polaron model [14,15], there is still no consensus about the type of quasiparticle effectively determining the electronic properties of doped STO and the mechanism of superconductivity. Several models were proposed, including pairing mediated by optical phonons [16,17], condensation of large polarons [18], or other exotic pairings in a Fermi liquid, such as the recent proposal of superconductivity mediated by ferroelectric fluctuations [19].

Here, we use high-resolution Ti L_3 edge resonant inelastic x-ray scattering (RIXS) to probe elementary low-energy excitations in insulating and conducting STO and LAO/STO heterostructures. We find that the electron-phonon coupling (EPC) to the longitudinal ~100 meV optical phonon mode, LO3, decreases as a function of the carrier density for both t_{2g} and e_g electrons. More importantly, we observe a ~130 meV composite excitation

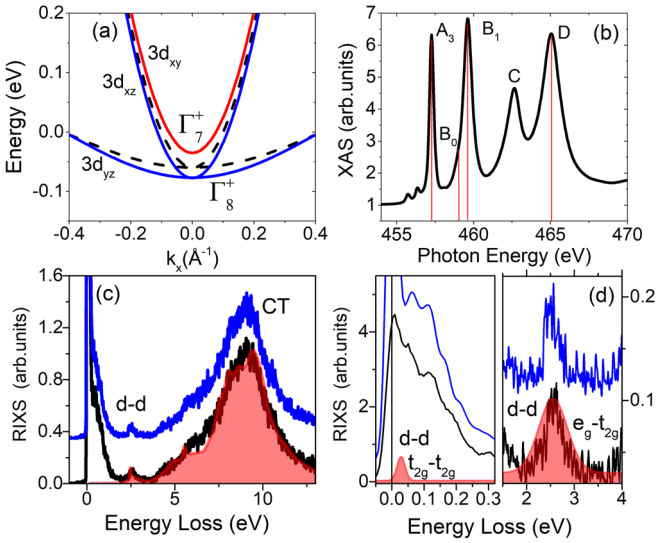

FIG. 1. Overview of x-ray absorption spectroscopy (XAS) and RIXS spectra: (a) Electronic structure of bulk STO derived from tight binding calculations [8] without (dashed black line) and with SOC (blue lines, Γ_8^+ quartet, red Γ_7^+ doublet). (b) XAS spectra on conducting bulk STO. (c) RIXS spectra at $B1$, normalized to the maximum of the charge transfer (CT) peak, for insulating STO (black line) and LAO/STO bilayer (blue line). The filled red shaded region is the calculated RIXS spectra using a BSE approach reproducing both *dd* (peak around 2.5 eV) and CT excitations. (d) Expanded view of the (left) low- and (right) midenergy regions, and atomic multiplet calculations including spin orbit interaction, which show the additional intra-t_{2g} *dd* peak around 30 meV.

assigned to an intra-t_{2g} *dd* transition accompanied by the emission of a LO3 phonon, providing evidence of large polaron quasiparticles in bulk STO and in the LAO/STO 2DEG.

RIXS spectra were measured at the beam line ID32 of the European Synchrotron Radiation Facility with the ERIXS setup [20]. The energy resolution, $\lesssim$35 meV (full width half maximum) as estimated from the nonresonant scattering by the silver contacts on the samples, was about 3 times better than in previous studies of Ti oxides [21–24], allowing a much deeper analysis of the results. We studied four types of samples with different carrier density, namely insulating and conducting STO single crystals, LAO/STO bilayers, and a LAO/STO multilayer (LAO/STO ML) composed by eight repetitions of a LAO(10 unit cells)/STO(10 unit cells) bilayer (see Table I and the Supplemental Material [25] for details). Following Ref. [33], the volume carrier densities n_{3D} of the LAO/STO samples were obtained from the measured 2D carrier density n_{2D} by considering the 2DEG effective thickness at the interface to be $d = 8.5 \pm 1.5$ nm, equal to the average of the experimental values reported in Refs. [33,34]. The RIXS spectra were acquired at 20 K excited at selected photon energies across the Ti L_3 edge and labeled $A3$, $B0$

TABLE I. Summary of the sample types studied in this Letter and their 10 K carrier density and resistivity.

Sample	n_{3D} (cm^{-3})	ρ (mΩcm)
STO insulating	$< 10^{15}$	$> 10^5$
STO conducting	5×10^{19}	0.2
LAO/STO bilayer	$2–4 \times 10^{19}$	0.4–0.5
LAO/STO multilayer	$0.5–1 \times 10^{21}$	0.01

(1.6 eV above $A3$), and $B1$ as shown in Fig. 1(b). In a simplified scenario for a Ti^{4+} ion in $3d^0$ configuration, the $A3$ and $B1$ absorption peaks correspond to the excitation of a $2p_{3/2}$ core electron into a $3d$ state of t_{2g} and e_g symmetry, respectively. The $B0$ energy, apparently at the bottom of a valley in the absorption spectrum of STO, corresponds to a peak for a Ti^{3+} ion in $3d^1$ configuration [9,10]. The incident photon polarization was perpendicular to the scattering plane (σ-pol) and the scattering angle 149.5°, at grazing incidence on the sample surface, corresponding to the $(-0.2, 0, 0.2)$ point in the reciprocal lattice.

A typical RIXS spectrum at $B1$ consists of a broad CT band between 4 and 14 eV, a very narrow peak around 2.5 eV due to interband *dd* transitions, and low-energy excitations, such as phonons, near the elastic peak [Figs. 1(c) and 1(d)]. The *dd* feature around 2.5 eV is observed in all the samples, even in the (nominally) undoped and insulating STO bulk single crystal, suggesting the presence of some $3d^1$ (Ti^{3+}) electrons [35]. The shape and relative intensities of the *dd* excitation and the CT peaks for the insulating STO spectra are very well reproduced by RIXS cross section calculations, based on the Bethe-Salpeter equation (BSE) [36], that consider both $3d^0$ and $3d^1$ contributions in a 20 to 1 ratio. In order to evaluate the role of SOC on the multiplet spectra, we used atomic multiplet calculations assuming the same fraction of $3d^1$ [Fig. 1(d)], which predicts an additional intra-t_{2g} *dd* peak around 30 meV energy loss, but no other feature up to 2.5 eV (see Ref. [25]).

Figure 2 shows typical low-energy loss RIXS data on insulating and conducting bulk STO for excitations at the $A3$, $B0$, and $B1$ energies. Three main features can be identified in the $A3$ and $B1$ spectra [Fig. 2(d)]: at low, intermediate, and high energies of 25–30 (ω_1), 55–65 (ω_2), and 90–100 meV (ω_3), respectively. As shown in Fig. 2(e), where we report the computed data of Ref. [37], these energies match the phonon branches of longitudinal (transverse) optical modes, namely LO1 (TO2), LO2 (TO3), and LO3 [38,39]. Besides the three main phonon peaks, several additional higher-energy features are visible in the data, some of them occurring at multiples of ω_3 ($\sim$200 and 300 meV), which correspond to two- and three- LO3 phonon replicas. Moreover, in the spectra at $B1$ and at $B0$, an additional particularly strong peak is visible around 125–135 meV in both insulating and conducting samples.

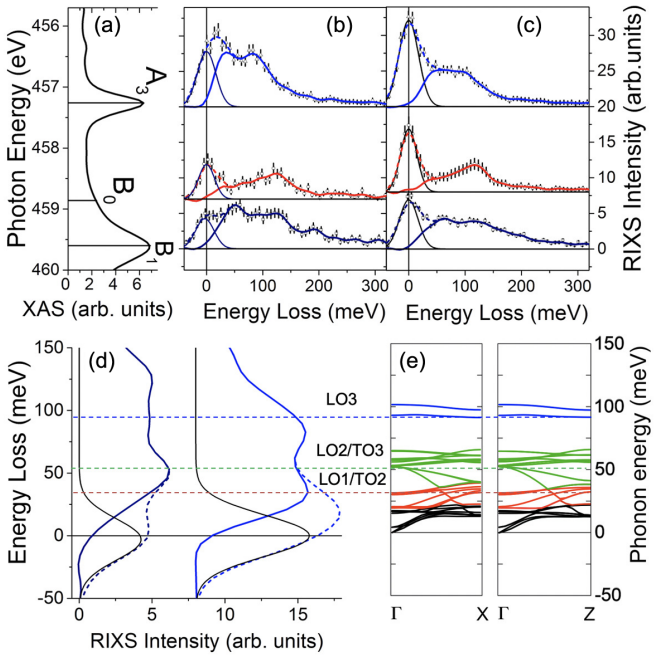

FIG. 2. Low-energy excitation RIXS spectra: (a) XAS spectrum around Ti L_3 edge of STO. (b),(c) RIXS data as function of incoming photon energy along the XAS Ti L_3 absorption edge for bulk (b) insulating and (c) conducting STO. For each energy, we show the raw scatter data, the elastic peak fit (black lines), and a 2 points fast Fourier transform (FFT) smoothing of the raw (short dashed lines) and elastic contribution subtracted data (solid lines). Different colors correspond to different photon energies, namely $A3$ (blue), $B0$ (red), and $B1$ (dark blue) (from top to bottom). The elastic peak has been determined by fixing the instrumental resolution from reference spectra on silver. (d) 2 points FFT smoothed raw (dashed lines) and elastic subtracted (solid lines) data at $A3$ (blue) and $B1$ (dark blue) for the STO insulating sample. Dashed horizontal lines indicate the three main phonon peaks compared to (e) tabulated STO phonon dispersions [37].

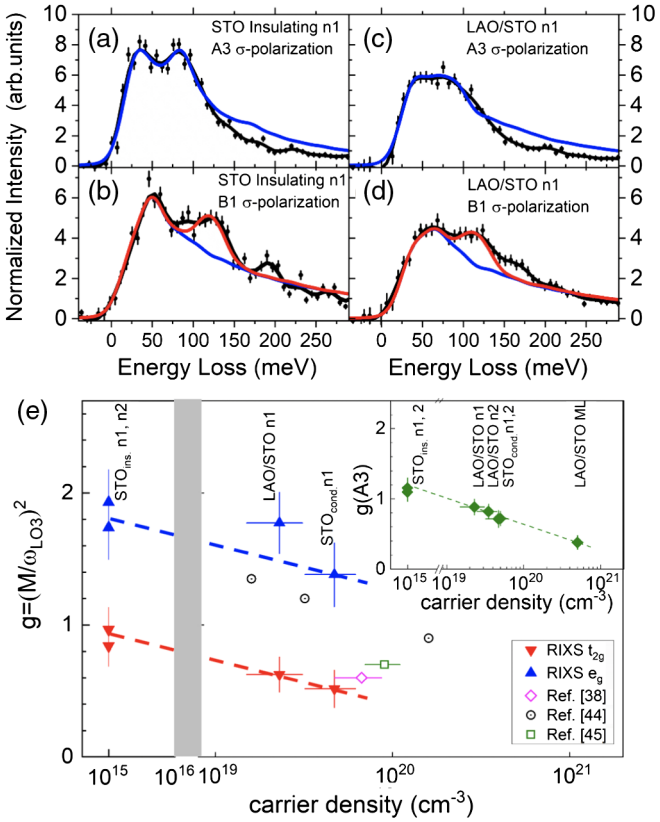

FIG. 3. Fit of the RIXS spectra. Comparison between RIXS data (black circles) of insulating STO [(a),(b)] and conducting LAO/STO [(c),(d)] and their fit at $A3$ (upper) and $B1$ (lower). Black lines are 2 point FFT smoothing of the data. Blue lines are the fit using the phonon mixing model. Red lines are the fit including the intra-t_{2g} dd plus LO3 phonon RIXS cross section of Eq. (1). (e) LO3 $g(t_{2g})$ (red triangles) and $g(e_g)$ (blue triangles) EPC estimated from the analysis of the RIXS data at $A3$ and $B1$ as function of the carrier density n_{3D}. The results are compared to data from Refs. [38,44,45]. The n_{3D} error bars for 2DEGs data are determined from the 2DEG thickness uncertainty. The shaded gray area is a break in the horizontal axis between 2×10^{16} and 8×10^{18} cm^{-3}. The inset shows $g(A3)$ as function of n_{3D} for all the samples studied. $n1$ and $n2$ designate different samples of the same type. Dashed lines are guides for eyes.

The data show strong differences in the low-energy spectra at $A3$ and $B1$, where phonons are expected to couple mainly to the t_{2g} and e_g electrons, respectively. In order to determine the t_{2g} and e_g coupling strengths ($g_{t_{2g}}$ and g_{e_g}, respectively), it is necessary to take into account that the $A3$ ($B1$) XAS peak has not a pure $2p^5 3dt_{2g}^1$ ($2p^5 3de_g^1$) character, but rather contains an approximate 25% mixing of e_g (t_{2g}) orbital character [39,40]. Because of the above points, we performed simultaneous constrained fits of the $A3$ and $B1$ RIXS spectra, employing a three-mode generalization of the Franck-Condon model [41]. The model, described in detail in Refs. [25,42], considers intermediate and final states containing not only multiples of a single mode but also mixed-mode double excitations. The Ti $2p$ core-hole lifetime Γ was fixed to 110 meV (HWHM) for both $A3$ and $B1$ spectra [43] (see Ref. [25] for an analysis of the Ti $2p$ core-hole lifetime).

In Figs. 3(a)–3(d) we show the fits at $A3$ and $B1$ for insulating bulk STO and a LAO/STO bilayer (other data fit on different samples and a complete list of the fitting parameters are shown in Supplemental Material [25]). We underline that most of the spectral weight above 100 meV and the very long tail in the data (extending above 0.5 eV) cannot be reproduced without considering phonon mixed excitations [25]. This indicates the importance of using a mixed phonon model for a better fitting when two or more phonons have comparable electron-phonon coupling and energies. We find $g_{e_g} > g_{t_{2g}}$ as a consequence of the larger spatial overlap of e_g orbitals with neighboring oxygen $2p$ states leading to σ bonds with respect to the π bond forming t_{2g} states. In Fig. 3(e), we show the LO3 electron-phonon coupling obtained from our RIXS data as function of the

volume carrier density reported in Table I and other experimental data collected from literature [38,44,45]. In order to compare bulk and 2DEGs data, we assigned a doping of 1×10^{15} cm^{-3} to the insulating STO, while n_{3D} for LAO/STO [38] and STO [45] 2DEGs is obtained from the reported n_{2D} using the value $d = 8.5 \pm 1.5$ nm for the 2DEG thickness. The analysis shows that the LO3 $g_{t_{2g}}$ EPC found by RIXS is in reasonable quantitative agreement with ARPES data reported on LAO/STO [38] and STO [45] samples with similar doping, and that it decreases as function of the carrier density, a result consistent with the dynamical screening of large polaron quasiparticles self polarization. This trend is confirmed in the carrier density dependence of the LO3 EPC determined from the fit of the RIXS spectra at $A3$ on all the STO and LAO/STO samples [see inset of Fig. 3(e)]. In particular, in the LAO/STO multilayer that hosts the highest carrier density among our samples, we obtain $g(A3) \simeq 0.4$, consistent with the bare undressed EPC of doped STO.

Although of fairly good quality for the general features, the fitting cannot account for the extra peak measured at ~130 meV in the $B0$ and $B1$ spectra, a feature that can even be stronger than the single phonon features. Evidently, it cannot be reproduced by the phonon mixing model and cannot be assigned to a multiple phonon replica. A pure dd excitation is also unlikely, as it would correspond to an unseemly large energy splitting of the t_{2g} states even in bulk STO. On the contrary, its energy is consistent with a composite excitation of an intra-t_{2g} transition for electrons in $3d^1$ Ti orbitals and one high-energy (90–100 meV) LO3 optical phonon. This is expected in a system where electrons get dressed by the polar distortions of the lattice, thus forming polarons.

In order to verify this idea, we included in the fit the RIXS cross section from a composite dd plus LO3 (ω_3) phonon excitation given, following Ref. [46], by

$$\frac{d^2\sigma}{dEd\Omega} = \frac{|T_{dd}|^2}{\Gamma^2} e^{-g_{dd}} \sum_{n=1}^{\infty} \frac{{g_{dd}}^n}{n!} \delta(E - E_{dd} - n\hbar\omega_3), \quad (1)$$

where T_{dd} is the polarization factor corresponding to the specific dd excitation and $g_{dd} = (M_{dd}/\omega_3)^2$ is the coupling constant, with M_{dd} half of the Jahn-Teller energy E_{JT}. As shown in Figs. 3(b)–3(d), a very satisfactory fitting of the data is obtained by only adjusting the value of g_{dd} and a scaling factor [inclusive of the term $|T_{dd}|^2$ in Eq. (1)], without changing the phonon-related part.

A further confirmation of this analysis comes from a fit of the $B0$ RIXS spectra. Here, the ~130 meV peak is enhanced with respect to pure phonon excitations, because $B0$ is a resonant transition for $3d^1$ states. We are able to fit the $B0$ RIXS spectra on each sample by using the same fitting parameters as at $B1$ and adjusting only the relative scaling factor for the pure phonon and the dd + LO3 phonon composite contributions (Fig. 4). The value of g_{dd} obtained from the fit at $B0$ and at $B1$ is 0.35 (0.32) for insulating (conductive) STO leads to $E_{JT} \simeq 105$ meV, in rough agreement with the theoretical estimations for STO [39] and $BaTiO_3$ [47]. The same analysis on the highly doped LAO/STO multilayer, characterized by a coupling to the LO3 mode of the order of the bare, undressed EPC shows that at high carrier density the ~130 meV feature is much weaker (Fig. 4). Indeed, from the fit at $B0$ we get a much smaller $g_{dd} \simeq 0.03$.

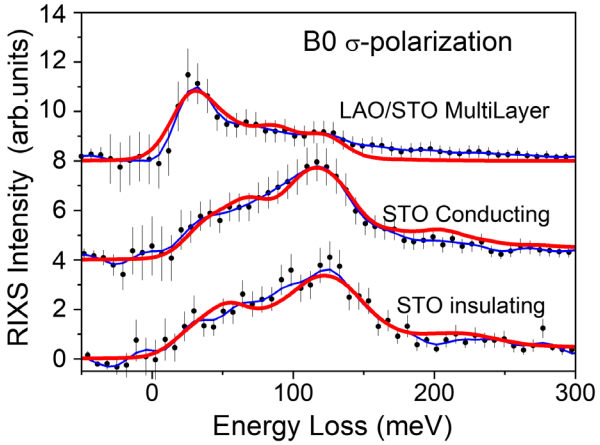

FIG. 4. Fit of the RIXS data at $B0$ (scatter data) for STO insulating, STO conducting, and highly doped LAO/STO multilayer, vertically displaced for clarity. Red lines are the fitting curves, while blue lines are 2 points FFT smoothed data.

While RIXS spectra in general can evolve as function of the carrier density also due to the electron coupling, alternative explanations of the suppression of the ~130 meV peak with doping are unlikely. In fact, we note that the increase of electron correlation and of the $3d$ population, both resulting from higher doping, would lead to larger, not lower, intensities of dd excitation features in RIXS. This rules out the assignment of the peak to pure dd excitations. On the contrary, we posit that at high carrier densities the intra-t_{2g} excitations do not induce anymore the emission of LO3 phonons because their coupling to the polar distortion of the lattice get too small. This phenomenology speaks strongly for the ~130 meV peak to be a hallmark of large polaron quasiparticles in insulating and weakly doped STO systems.

Our results have several implications. High-resolution RIXS spectra not only quantify trends in the EPC for optical phonons, they also reveal polaronic excitations in bulk STO and STO-based heterostructures, demonstrating that RIXS can be used to study polaron physics both in insulating and conducting materials. We note that a ~130 meV feature was observed in optical conductivity data of doped STO [14] and recently explained within a large polaron model by the inclusion of the dynamical screening of electrons from the lattice polarization [15]. The coincidence in energy position and carrier density

dependence, with a disappearance at high doping, suggests that RIXS and optical conductivity observations have a common origin. Furthermore, by RIXS we have shown that the ∼130 meV peak involves *dd* intra-t_{2g} transitions of $3d^1$ Ti^{3+} states, accompanied by the excitation of LO3 phonons. Consequently, t_{2g} electrons in STO form large polaron quasiparticles. Beside confirming earlier signatures by ARPES at the surface of STO [45], in LAO/STO [38] and in FeSe/STO bilayers [5], our study demonstrates more generally the emergence of large polaron physics in both bi- and three-dimensional titanates. Finally, it emerges that polarons are observed also in nominally undoped STO, with a coupling constant well below the value expected for small polarons formation. Consequently, we can infer that even at the very low doping level, as that induced by residual defects or by long living photodoped carriers, $3d^1$ electrons are dressed by long-range polar lattice distortions, as theoretically predicted in other wide band gap materials like LiF [48]. Future investigations and theoretical modeling of the normal and superconducting state of STO and STO-based heterostructures will have to take in consideration the central role of large polarons in these materials.

The authors gratefully acknowledge the help of the ID32 beam line staff at ESRF. This project received funding from the EU Horizon H2020 project QUANTOX (Grant No. 731473); MIUR of Italy for the PRIN projects TOPSPIN (Grant No. PRIN 20177SL7HC), and QUANTUM 2D (Grant No. PRIN 2017Z8TS5B); from the Fondazione CARIPLO and Regione Lombardia for the ERC-P-ReXS project (Grant No. 2016-0790). K. G. was supported by the U.S. Department of Energy, Office of Science, Basic Energy Sciences as part of the Computational Materials Science Program.

*marco.salluzzo@spin.cnr.it
†Present address: Max Planck Institut für Festkörperforschung, Heisenbergstrasse 1, D-70569 Stuttgart, Germany.

[1] A. Ohtomo and H. Y. Hwang, A high-mobility electron gas at the $LaAlO_3/SrTiO_3$ heterointerface, Nature (London) **427**, 423 (2004).
[2] N. Reyren, S. Thiel, A. D. Caviglia, L. F. Kourkoutis, G. Hammerl, C. Richter, C. W. Schneider, T. Kopp, A.-S. Rüetschi, D. Jaccard, M. Gabay, D. A. Muller, J.-M. Triscone, and J. Mannhart, Superconducting interfaces between insulating oxides, Science **317**, 1196 (2007).
[3] D. Di Castro, M. Salvato, A. Tebano, D. Innocenti, C. Aruta, W. Prellier, O. I. Lebedev, I. Ottaviani, N. B. Brookes, M. Minola, M. Moretti Sala, C. Mazzoli, P. G. Medaglia, G. Ghiringhelli, L. Braicovich, M. Cirillo, and G. Balestrino, Occurrence of a high-temperature superconducting phase in $(CaCuO_3)_n/(SrTiO_3)_m$(cacuo2)n/(srtio3)m superlattices, Phys. Rev. B **86**, 134524 (2012).
[4] Q.-Y. Wang, Z. Li, W.-H. Zhang, Z.-C. Zhang, J.-S. Zhang, W. Li, H. Ding, Y.-B. Ou, P. Deng, K. Chang, J. Wen, C.-L. Song, K. He, J.-F. Jia, S.-H. Ji, Y.-Y. Wang, L.-L. Wang, X. Chen, X.-C. Ma, and Q.-K. Xue, Interface-induced high-temperature superconductivity in single unit-cell FeSe Films on $SrTiO_3$, Chin. Phys. Lett. **29**, 037402 (2012).
[5] J.-F. Ge, Z.-L. Liu, C. Liu, C.-L. Gao, D. Qian, Q.-K. Xue, Y. Liu, and J.-F. Jia, Superconductivity above 100 K in single-layer FeSe films on doped $SrTiO_3$, Nat. Mater. **14**, 285 (2015).
[6] J. J. Lee, F. T. Schmitt, R. G. Moore, S. Johnston, Y.-T. Cui, W. Li, M. Yi, Z. K. Liu, M. Hashimoto, Y. Zhang, D. H. Lu, T. P. Devereaux, D.-H. Lee, and Z.-X. Shen, Interfacial mode coupling as the origin of the enhancement of T_c in FeSe films on $SrTiO_3$, Nature (London) **515**, 245 (2014).
[7] L. F. Mattheiss, Effect of the 110°K phase transition on the $SrTiO_3$ conduction bands, Phys. Rev. B **6**, 4740 (1972).
[8] Z. Zhong, A. Tóth, and K. Held, Theory of spin-orbit coupling at $LaAlO_3/SrTiO_3$ interfaces and $SrTiO_3$ surfaces, Phys. Rev. B **87**, 161102(R) (2013).
[9] M. Salluzzo, J. C. Cezar, N. B. Brookes, V. Bisogni, G. M. De Luca, C. Richter, S. Thiel, J. Mannhart, M. Huijben, A. Brinkman, G. Rijnders, and G. Ghiringhelli, Orbital Reconstruction and the Two-Dimensional Electron Gas at the $LaAlO_3/SrTiO_3$ Interface, Phys. Rev. Lett. **102**, 166804 (2009).
[10] C. Cancellieri, M. L. Reinle-Schmitt, M. Kobayashi, V. N. Strocov, P. R. Willmott, D. Fontaine, P. Ghosez, A. Filippetti, P. Delugas, and V. Fiorentini, Doping-dependent band structure of $LaAlO_3/SrTiO_3$ interfaces by soft x-ray polarization-controlled resonant angle-resolved photoemission, Phys. Rev. B **89**, 121412(R) (2014).
[11] J. L. M. van Mechelen, D. van der Marel, C. Grimaldi, A. B. Kuzmenko, N. P. Armitage, N. Reyren, H. Hagemann, and I. I. Mazin, Electron-Phonon Interaction and Charge Carrier Mass Enhancement in $SrTiO_3$, Phys. Rev. Lett. **100**, 226403 (2008).
[12] D. van der Marel, J. L. M. van Mechelen, and I. I. Mazin, Common Fermi-liquid origin of T^2 resistivity and superconductivity in *n*-type $SrTiO_3$, Phys. Rev. B **84**, 205111 (2011).
[13] W. Meevasana, X. J. Zhou, B. Moritz, C.-C. Chen, R. H. He, S.-I. Fujimori, D. H. Lu, S.-K. Mo, R. G. Moore, F. Baumberger, T. P. Devereaux, D. van der Marel, N. Nagaosa, J. Zaanen, and Z.-X. Shen, Strong energy–momentum dispersion of phonon-dressed carriers in the lightly doped band insulator $SrTiO_3$, New J. Phys. **12**, 023004 (2010).
[14] J. T. Devreese, S. N. Klimin, J. L. M. van Mechelen, and D. van der Marel, Many-body large polaron optical conductivity in $SrTi_{1-x}Nb_xO_3$, Phys. Rev. B **81**, 125119 (2010).
[15] S. Klimin, J. Tempere, J. T. Devreese, C. Franchini, and G. Kresse, Optical response of an interacting polaron gas in strongly polar crystals, Appl. Sci. **10**, 2059 (2020).
[16] A. Baratoff and G. Binnig, Mechanism of superconductivity in $SrTiO_3$, Physica (Amsterdam) **108(B+C)**, 1335 (1981).
[17] J. Appel, Soft-mode superconductivity in $SrTiO_{3-x}$, Phys. Rev. **180**, 508 (1969).
[18] S. N. Klimin, J. Tempere, J. T. Devreese, and D. van der Marel, Interface superconductivity in $LaAlO_3 - SrTiO_3$ heterostructures, Phys. Rev. B **89**, 184514 (2014).
[19] J. M. Edge, Y. Kedem, U. Aschauer, N. A. Spaldin, and A. V. Balatsky, Quantum Critical Origin of the

Superconducting Dome in $SrTiO_3$, Phys. Rev. Lett. **115**, 247002 (2015).

[20] N. Brookes, F. Yakhou-Harris, K. Kummer, A. Fondacaro, J. Cezar, D. Betto, E. Velez-Fort, A. Amorese, G. Ghiringhelli, L. Braicovich, R. Barrett, G. Berruyer, F. Cianciosi, L. Eybert, P. Marion, P. van der Linden, and L. Zhang, The beamline ID32 at the ESRF for soft X-ray high energy resolution resonant inelastic X-ray scattering and polarisation dependent X-ray absorption spectroscopy, Nucl. Instrum. Methods Phys. Res., Sect. A **903**, 175 (2018).

[21] S. Moser, S. Fatale, P. Krüger, H. Berger, P. Bugnon, A. Magrez, H. Niwa, J. Miyawaki, Y. Harada, and M. Grioni, Electron-Phonon Coupling in the Bulk of Anatase TiO_2 Measured by Resonant Inelastic X-Ray Spectroscopy, Phys. Rev. Lett. **115**, 096404 (2015).

[22] S. Fatale, S. Moser, J. Miyawaki, Y. Harada, and M. Grioni, Hybridization and electron-phonon coupling in ferroelectric $BaTiO_3$ probed by resonant inelastic x-ray scattering, Phys. Rev. B **94**, 195131 (2016).

[23] K.-J. Zhou, M. Radovic, J. Schlappa, V. Strocov, R. Frison, J. Mesot, L. Patthey, and T. Schmitt, Localized and delocalized Ti $3d$ carriers in $LaAlO_3/SrTiO_3$ superlattices revealed by resonant inelastic x-ray scattering, Phys. Rev. B **83**, 201402(R) (2011).

[24] F. Pfaff, H. Fujiwara, G. Berner, A. Yamasaki, H. Niwa, H. Kiuchi, A. Gloskovskii, W. Drube, J. Gabel, O. Kirilmaz, A. Sekiyama, J. Miyawaki, Y. Harada, S. Suga, M. Sing, and R. Claessen, Raman and fluorescence contributions to the resonant inelastic soft x-ray scattering on $LaAlO_3/SrTiO_3$ heterostructures, Phys. Rev. B **97**, 035110 (2018).

[25] See Supplemental Material at http://link.aps.org/supplemental/10.1103/PhysRevLett.125.126401 for details on the models used to fit the data, supplementary fitting curves (Fig. S1) and Table S1, an analysis on the core-hole lifetime Γ (Fig. S2 and Table S2), and transport data on the samples (Fig. S3), which includes Refs. [26–32].

[26] P. Sałek, F. Gel'mukhanov, H. Ågren, O. Björneholm, and S. Svensson, Generalized Franck-Condon principle for resonant photoemission, Phys. Rev. A **60**, 2786 (1999).

[27] P. Giannozzi *et al.*, QUANTUM ESPRESSO: a modular and open-source software project for quantum simulations of materials, J. Phys. Condens. Matter **21**, 395502 (2009).

[28] Y. L. Wang, G. Fabbris, M. P. M. Dean, and G. Kotliar, EDRIXS: An open source toolkit for simulating spectra of resonant inelastic x-ray scattering, Comput. Phys. Commun. **243**, 151 (2019).

[29] R. D. Cowan, *The Theory of Atomic Structure and Spectra*, Los Alamos Series in Basic and Applied Sciences (University of California Press, Ltd., Berkeley, 1981).

[30] M. Kawasaki, K. Takahashi, T. Maeda, R. Tsuchiya, M. Shinohara, O. Ishiyama, T. Yonezawa, M. Yoshimoto, and H. Koinuma, Atomic control of the $SrTiO_3$ crystal surface, Science **266**, 1540 (1994).

[31] G. Koster, B. L. Kropman, G. J. Rijnders, D. H. Blank, and H. Rogalla, Quasi-ideal strontium titanate crystal surfaces through formation of strontium hydroxide, Appl. Phys. Lett. **73**, 2920 (1998).

[32] A. Fragneto, G. M. De Luca, R. Di Capua, U. Scotti di Uccio, M. Salluzzo, X. Torrelles, T.-L. Lee, and J. Zegenhagen, Ti- and Sr-rich surfaces of $SrTiO_3$ studied by grazing incidence x-ray diffraction, Appl. Phys. Lett. **91**, 101910 (2007).

[33] S. Gariglio, M. Gabay, J. Mannhart, and J. M. Triscone, Interface superconductivity, Physica (Amsterdam) **514C**, 189 (2015).

[34] M. Basletic, J. L. Maurice, C. Carrétéro, G. Herranz, O. Copie, M. Bibes, E. Jacquet, K. Bouzehouane, S. Fusil, and A. Barthélémy, Mapping the spatial distribution of charge carriers in $LaAlO_3/SrTiO_3$ heterostructures, Nat. Mater. **7**, 621 (2008).

[35] Ti^{3+} in bulk STO can be due to residual defects and/or long-living photodoped carriers promoted from shallow energy traps under the beam irradiation.

[36] K. Gilmore, J. Vinson, E. Shirley, D. Prendergast, C. Pemmaraju, J. Kas, F. Vila, and J. Rehr, Efficient implementation of core-excitation Bethe–Salpeter equation calculations, Comput. Phys. Commun. **197**, 109 (2015).

[37] G. Petretto, S. Dwaraknath, H. P. C. Miranda, D. Winston, M. Giantomassi, M. J. van Setten, X. Gonze, K. A. Persson, G. Hautier, and G.-M. Rignanese, High-throughput density-functional perturbation theory phonons for inorganic materials, Sci. Data **5**, 180065 (2018); H. P. C. Miranda and L. Writz, Theor. Solid State Phys., Home, http://henriquemiranda.github.io/phononwebsite/ (2014).

[38] C. Cancellieri, A. S. Mishchenko, U. Aschauer, A. Filippetti, C. Faber, O. S. Barisic, V. A. Rogalev, T. Schmitt, N. Nagaosa, and V. N. Strocov, Polaronic metal state at the $LaAlO_3/SrTiO_3$ interface, Nat. Commun. **7**, 10386 (2016).

[39] K. Gilmore and E. L. Shirley, Numerical quantification of the vibronic broadening of the $SrTiO_3$ Ti L-edge spectrum, J. Phys. Condens. Matter **22**, 315901 (2010).

[40] K. Ogasawara, T. Iwata, Y. Koyama, T. Ishii, I. Tanaka, and H. Adachi, Relativistic cluster calculation of ligand-field multiplet effects on cation $L_{2,3}$ x-ray-absorption edges of $SrTiO_3$, NiO, and CaF_2, Phys. Rev. B **64**, 115413 (2001).

[41] L. J. P. Ament, M. van Veenendaal, and J. van den Brink, Determining the electron-phonon coupling strength from Resonant Inelastic X-ray Scattering at transition metal L-edges, Europhys. Lett. **95**, 27008 (2011).

[42] A. Geondzhian and K. Gilmore, Generalization of the Franck-Condon model for phonon excitations by resonant inelastic x-ray scattering, Phys. Rev. B **101**, 214307 (2020).

[43] M. O. Krause and J. H. Oliver, Natural widths of atomic K and L levels, $K\alpha$ X-ray lines and several KLL Auger lines, J. Phys. Chem. Ref. Data **8**, 329 (1979).

[44] A. G. Swartz, H. Inoue, T. A. Merz, Y. Hikita, S. Raghu, T. P. Devereaux, S. Johnston, and H. Y. Hwang, Polaronic behavior in a weak-coupling superconductor, Proc. Natl. Acad. Sci. U.S.A. **115**, 1475 (2018).

[45] Z. Wang, S. McKeown Walker, A. Tamai, Y. Wang, Z. Ristic, F. Y. Bruno, A. de la Torre, S. Riccò, N. C. Plumb, M. Shi, P. Hlawenka, J. Sánchez-Barriga, A. Varykhalov, T. K. Kim, M. Hoesch, P. D. C. King, W. Meevasana, U. Diebold, J. Mesot, B. Moritz, T. P. Devereaux, M. Radovic, and F. Baumberger, Tailoring the nature and strength of

electron–phonon interactions in the $SrTiO_3(001)$ 2D electron liquid, Nat. Mater. **15**, 835 (2016).

[46] L. J. P. Ament, Resonant inelastic x-ray scattering studies of elementary excitations, Casimir Ph.D. Series, Leiden University, Faculty of Science, 2010, http://hdl.handle.net/1887/16138.

[47] I. B. Bersuker, Pseudo Jahn–Teller effect in the origin of enhanced flexoelectricity, Appl. Phys. Lett. **106**, 022903 (2015).

[48] W. H. Sio, C. Verdi, S. Poncé, and F. Giustino, Polarons from First Principles, without Supercells, Phys. Rev. Lett. **122**, 246403 (2019).